Supporting Information for

Homoleptic Biisoquinolinedioxide Lanthanide Complexes for Near-Infrared Circularly Polarized Luminescence

Douglas Kariuki Mundia,[a] Ashley Schmidt,[b] Jerome R. Robinson,[c] Nathan D. Schley,[d] Gaël Ung[a,*]

[a] Department of Chemistry, University of Connecticut, Storrs, Connecticut 06269, United States.

[b] Brucker AXS LLC, Madison, Wisconsin 53711-5373, United States.

[c] Department of Chemistry, Brown University, Providence, RI 02912, United States.

[d] Department of Chemistry, Vanderbilt University, Nashville, Tennessee 37235, United States.

Email: gael.ung@uconn.edu

Table of Contents

General Methods and Materials

The ligand synthesis and resolution of enantiomers were carried out based on previously reported procedures.[1–3] All operations leading to ligand synthesis and resolution were performed under an inert atmosphere of nitrogen using standard Schlenk techniques unless otherwise stated. The lanthanide complexes and single crystals were prepared in a Vigor glovebox filled with nitrogen.

2,2,6,6-tetramethylpiperidine (TMPH, 99%) and *N*,*N*,*N*',*N*'-tetramethylethylenediamine (TMEDA, 99%) were purchased from Oakwood and Acros, respectively. Both reagents were dried using calcium hydride procured from Thermo Scientific (92% min) under nitrogen, then distilled under inert conditions before use. Butylmagnesium chloride (98%) was purchased from Sigma-Aldrich as a 2.0 M solution in tetrahydrofuran and was used as received. Isoquinoline (97%) was purchased from Thermo Scientific and purified by sublimation before use. 3-Chloroperoxybenzoic acid (70-75%) was purchased from Acros and used without further purification. (*R*)- and (*S*)-1,1'-binaphthalene-2,2'-diol (99%) were purchased from Ambeed and used as received. All solvents were HPLC grade (99.9%) and purchased from commercial suppliers. Toluene was further dried by refluxing under nitrogen in the presence of sodium metal for 12 hours before distilling under nitrogen. Tetrahydrofuran was further dried using a solvent purification system from Pure Process Technology. Erbium, yttrium, and ytterbium trifluoromethanesulfonates (98%) were purchased from Strem Chemicals and used as received without further purification.

NMR Spectroscopy

NMR spectra were recorded using either a Bruker AVANCE III 300 or 400 MHz spectrometer. Spectral data were processed and analyzed with MestReNova and Bruker TopSpin software packages. All chemical shifts are given in parts per million (ppm) relative to the residual solvent resonances: $CDCl_3$ (δ = 7.26 ppm for ^1H, 77.16 ppm for ^{13}C) and CD_3CN (δ = 1.94 ppm for ^1H, 1.3 ppm and 118.3 ppm for ^{13}C).

Photophysical Studies

UV–visible absorption, excitation, and emission spectra were obtained from 10^{-4} M solutions in 1,2-difluorobenzene using a HORIBA Duetta spectrometer, and data were processed with the accompanying EzSpec software suite.

Quantum yields were measured using the relative method with 3.5 mL quartz cuvettes as the sample holders. This involved collecting emission spectra on an OLIS NIR CPL Solo spectrofluorometer and absorbance spectra on a HORIBA Duetta spectrometer from dilute solutions prepared in acetonitrile. The starting point for these dilutions was a 10^{-6} M stock solution. Emission spectra were collected at 365 nm excitation with slit width set at 26 nm, while absorbance spectra were collected at 1 nm slit width. The reference standard employed was $[(binol)_3YbNa_3(thf)_6]$ (ϕ_f = 0.17 in THF).

Luminescence lifetimes were measured from 10^{-4} M 1,2-difluorobenzene solutions using the OLIS NIR CPL Solo spectrofluorometer. Decay profiles were obtained under pulsed excitation at 380

nm, monitoring the emission maximum. Excitation and emission slit widths were set to 26 nm for Yb-based emitters. The decay traces were fitted to a first-order monoexponential model to extract the observed fluorescence lifetimes (τ_{obs}) of the emissive components, reported as measured lifetime (observation wavelength).

Circular dichroism (CD) spectra were recorded from 10^{-4} M acetonitrile solutions of the complexes at ambient temperature using an Applied Photophysics PiStar spectropolarimeter with a 1 cm path length.

Circularly polarized luminescence (CPL) spectra and the corresponding g_{lum} values were collected using an OLIS NIR CPL Solo spectrofluorometer, and all data were processed using the OLIS GlobalWorks software package.

All measurements were carried out on an OLIS NIR CPL Solo instrument equipped with a Hamamatsu H10330C-75-C2 NIR photomultiplier tube (PMT) detector, a C9744 photon counter, and an integrated Peltier cooling unit (Hamamatsu Photonics K.K., Japan).

XRD Studies

The crystal structures were determined using a Bruker D8 VENTURE KAPPA single crystal X-ray diffractometer with a DIAMOND II hybrid anode microfocus source (λ = 0.71073 Å) using a multilayer mirror as the monochromator and a PHOTON III CPAD detector. All data were integrated with SAINT V8.42.[4] A Multi-Scan absorption correction using SADABS 2016/2 was applied.[5] The structure was solved by Intrinsic Phasing methods with SHELXT 2018/2 and refined by full-matrix least-squares methods against F2 using SHELXL-2019/2.[6,7] All atoms were refined with anisotropic displacement parameters. Crystallographic data for the structures reported in this paper have been deposited with the Cambridge Crystallographic Data Centre.[8] CCDC 2503942 contains the supplementary crystallographic data for this paper. This data can be obtained free of charge from The Cambridge Crystallographic Data Centre via www.ccdc.cam.ac.uk/structures. The CIF file was generated using FinalCif.[9]

Synthesis and Resolution of BIQNO

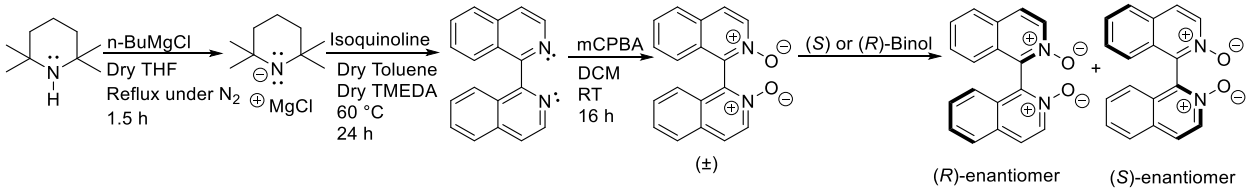

Synthesis of 1,1'-Biisoquinoline

A 250 mL three-neck reaction flask with a stir bar was fitted with a condenser, septum, and connected to a Schlenk line. The flask was flame-dried under vacuum and then allowed to cool to room temperature and put under nitrogen. 4 mL of dry TMPH (3.28 g, 23.2 mmol, 0.6 equiv) was added to the flask, followed by 21.6 mL of dry THF. 11.6 mL of 2M n-BuMgCl (23.23 mmol, 0.6 equiv) in THF was added, and the reaction was refluxed for 2 hours. THF was pumped off under vacuum, then 30 mL of dry toluene was added to the flask. 3.5 mL of dry TMEDA (2.7 g, 23.2

mmol, 0.6 equiv) was added to the flask, and the mixture was stirred for 30 min. 5 g of isoquinoline (38.71 mmol, 1 equiv) dissolved in 20 mL of dry toluene was added to the flask, and the mixture was stirred for 72 hours under nitrogen. After completion of the reaction, the mixture was cooled to 0° C, ice-cold water was added, and the mixture was stirred for 30 mins while open to air. The mixture was extracted with three 50 mL aliquots of dichloromethane. All organic layers were combined, washed with brine, and dried with anhydrous Na_2SO_4. The drying agent was removed by filtration, and the filtrate was concentrated under vacuum to give the crude product. The resulting product was purified by silica gel column chromatography with 30% EtOAc in hexane as the mobile phase to afford 2.18 g of yellow crystals (8.5 mmol, 44% yield).

^{1}H NMR (300 MHz, $CDCl_3$) δ 8.72 (d, *J* = 5.7 Hz, 2H), 7.95 (d, *J* = 8.3 Hz, 2H), 7.82 (dd, *J* = 5.7, 0.9 Hz, 2H), 7.79 – 7.67 (m, 4H), 7.48 (ddd, *J* = 8.3, 6.9, 1.2 Hz, 2H).

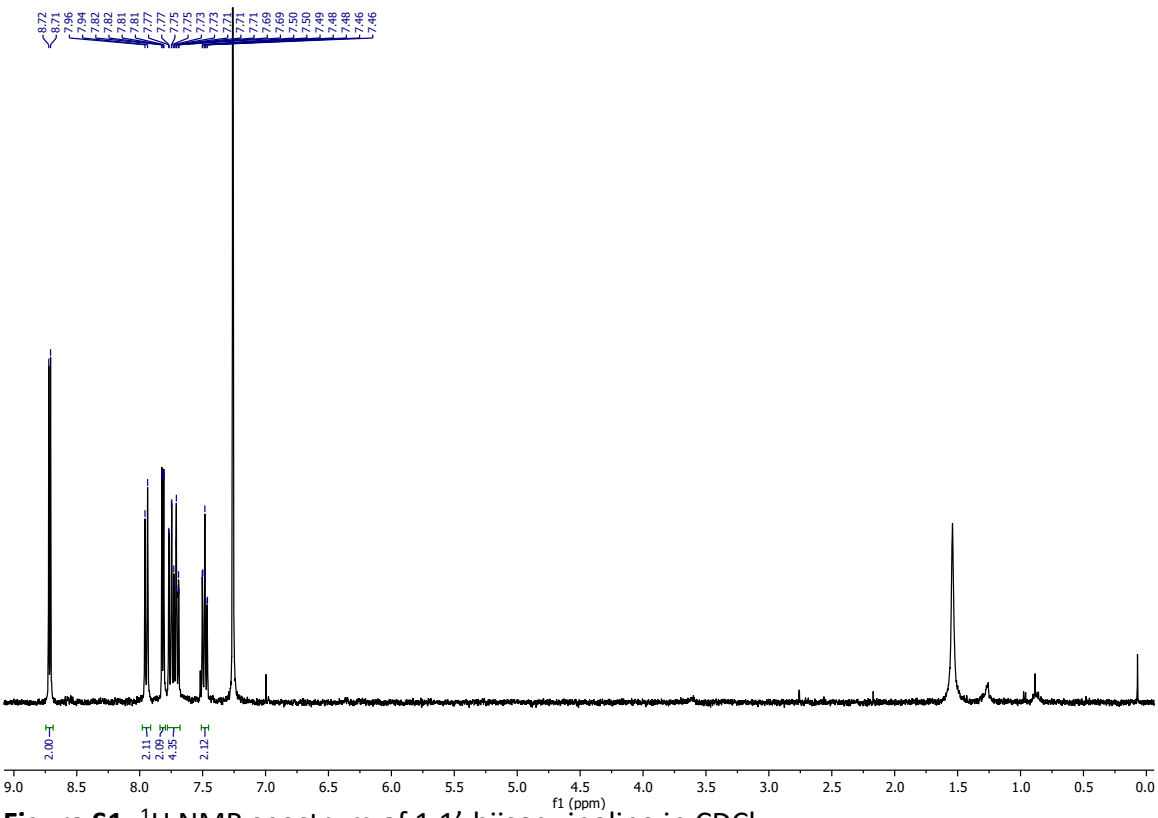

Figure S1: ^{1}H NMR spectrum of 1,1'-biisoquinoline in $CDCl_3$

Synthesis of 1,1'-biisoquinoline-*N,N'*-dioxide

1.7 g of 1,1'-biisoquinoline (6.6 mmol, 1 equiv) was dissolved in 20 mL of dichloromethane and transferred into a 100 mL Schlenk flask under nitrogen. 4.7 g of 70-75% meta-chloroperoxybenzoic acid (19 mmol, 3 equiv) dissolved in 30 mL dichloromethane was added dropwise into the flask at 0 °C. The resulting mixture was stirred for 16 h at room temperature. The reaction was quenched by adding dimethyl sulfide (1.5 mL, 19 mmol) and concentrated under vacuum. 50 mL of dichloromethane was then added to the flask to redissolve the contents and then transferred to a 250 mL separatory funnel. The organic layer was washed with three 50 mL aliquots of saturated $NaHCO_3$ and then washed with brine before drying with anhydrous Na_2SO_4.

The drying agent was removed, and the filtrate was concentrated under vacuum to give the crude product. The crude product was further purified by recrystallizing from hot ethanol to obtain 1.89 g of white crystals (6.6 mmol, 99% yield).

^{1}H NMR (300 MHz, $CDCl_3$) δ 8.34 (d, *J* = 7.2 Hz, 2H), 7.89 (d, *J* = 8.1 Hz, 2H), 7.85 (d, *J* = 7.2 Hz, 2H), 7.62 – 7.52 (m, 2H), 7.52 – 7.43 (m, 2H), 7.13 (dd, *J* = 8.4, 1.0 Hz, 2H).

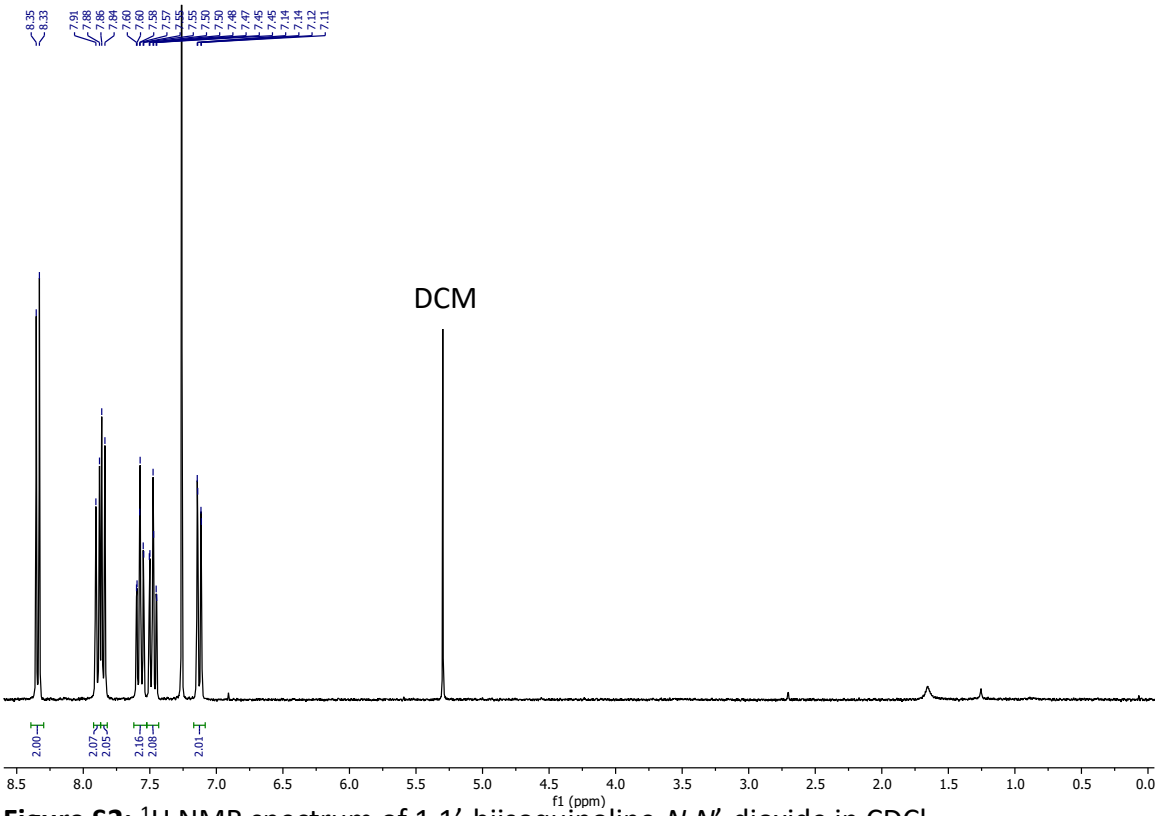

Figure S2: ^{1}H NMR spectrum of 1,1'-biisoquinoline-*N*,*N*'-dioxide in $CDCl_3$

Resolution of enantiomers

Racemic 1,1'-biisoquinoline-*N,N'*-dioxide (1.94 g, 6.73 mmol) was added to a 100 mL Schlenk flask, followed by (*R*)-1,1'-binaphthalene-2,2'-diol (1.93 g, 6.73 mmol), and then 50 mL of dichloromethane was added to the flask. The mixture was heated by a heat gun until all solids dissolved and allowed to cool to room temperature. The resultant solution was concentrated under vacuum to induce crystal growth and then allowed to stand for two days at room temperature to afford yellow crystals. The crystals were separated into optically pure (*S*)-1,1'-biisoquinoline-*N,N*'-dioxide (0.46 g, 1.60 mmol, 47% yield) and (*R*)-1,1'-binaphthalene-2,2'-diol by flash chromatography on silica gel with 2% methanol in dichloromethane as the eluent.

$[\alpha]_D^{22} - 180°$ (c 1.01, $CHCl_3$).

^{1}H NMR (300 MHz, $CDCl_3$) δ 8.34 (d, *J* = 7.2 Hz, 2H), 7.89 (d, *J* = 8.1 Hz, 2H), 7.85 (d, *J* = 7.2 Hz, 2H), 7.62 – 7.52 (m, 2H), 7.52 – 7.43 (m, 2H), 7.13 (dd, *J* = 8.4, 1.0 Hz, 2H).

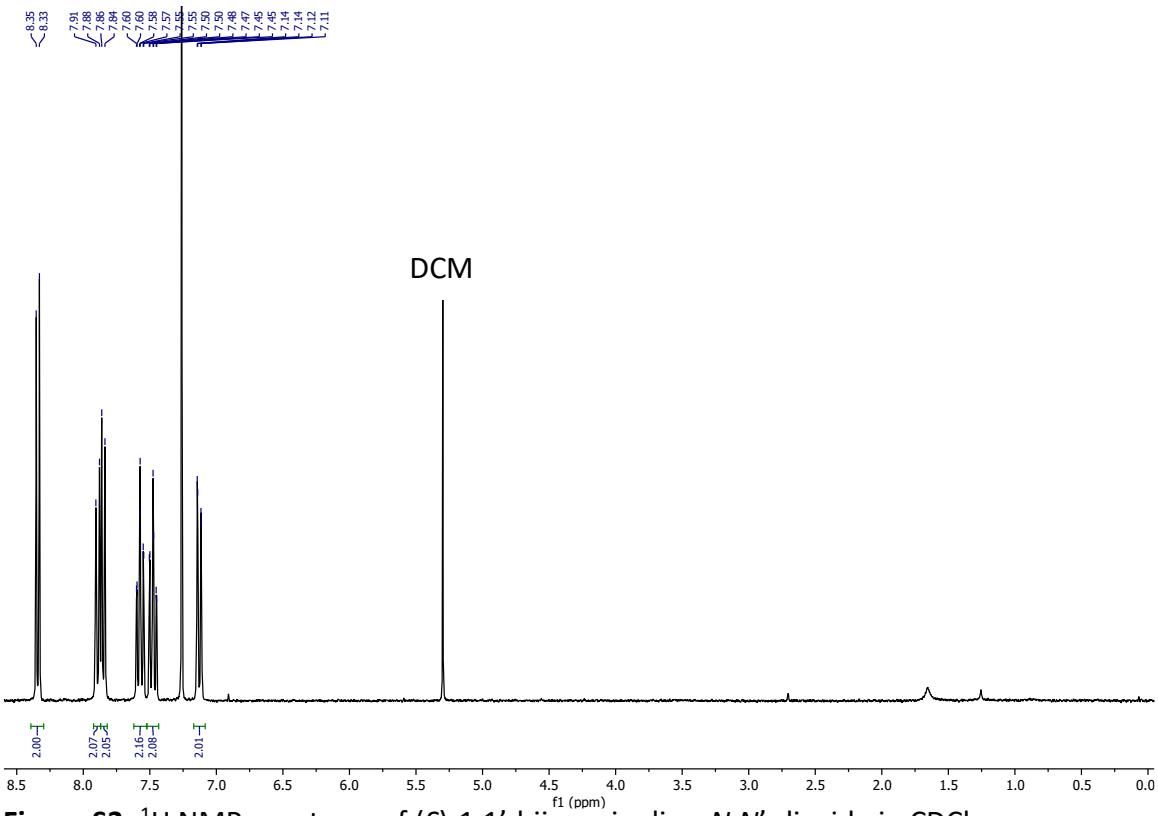

Figure S3: ^{1}H NMR spectrum of (*S*)-1,1'-biisoquinoline-*N*,*N*'-dioxide in $CDCl_3$

The mother liquor was concentrated under vacuum, and the residue was purified by flash chromatography to recover the (*R*)-1,1'-biisoquinoline-*N,N*'-dioxide enriched product and (*R*)-1,1'-binaphthalene-2,2'-diol. With the aid of (*S*)-1,1'-binaphthalene-2,2'-diol in the manner described above, optically pure (*R*)-1,1'-biisoquinoline-*N,N*'-dioxide was afforded (0.3 g, 1.04 mmol, 31% yield).

$[\alpha]_D^{22} + 179°$ (c 1.01, $CHCl_3$).

^{1}H NMR (300 MHz, $CDCl_3$) δ 8.34 (d, *J* = 7.2 Hz, 2H), 7.89 (d, *J* = 8.1 Hz, 2H), 7.85 (d, *J* = 7.2 Hz, 2H), 7.62 – 7.52 (m, 2H), 7.52 – 7.43 (m, 2H), 7.13 (dd, *J* = 8.4, 1.0 Hz, 2H).

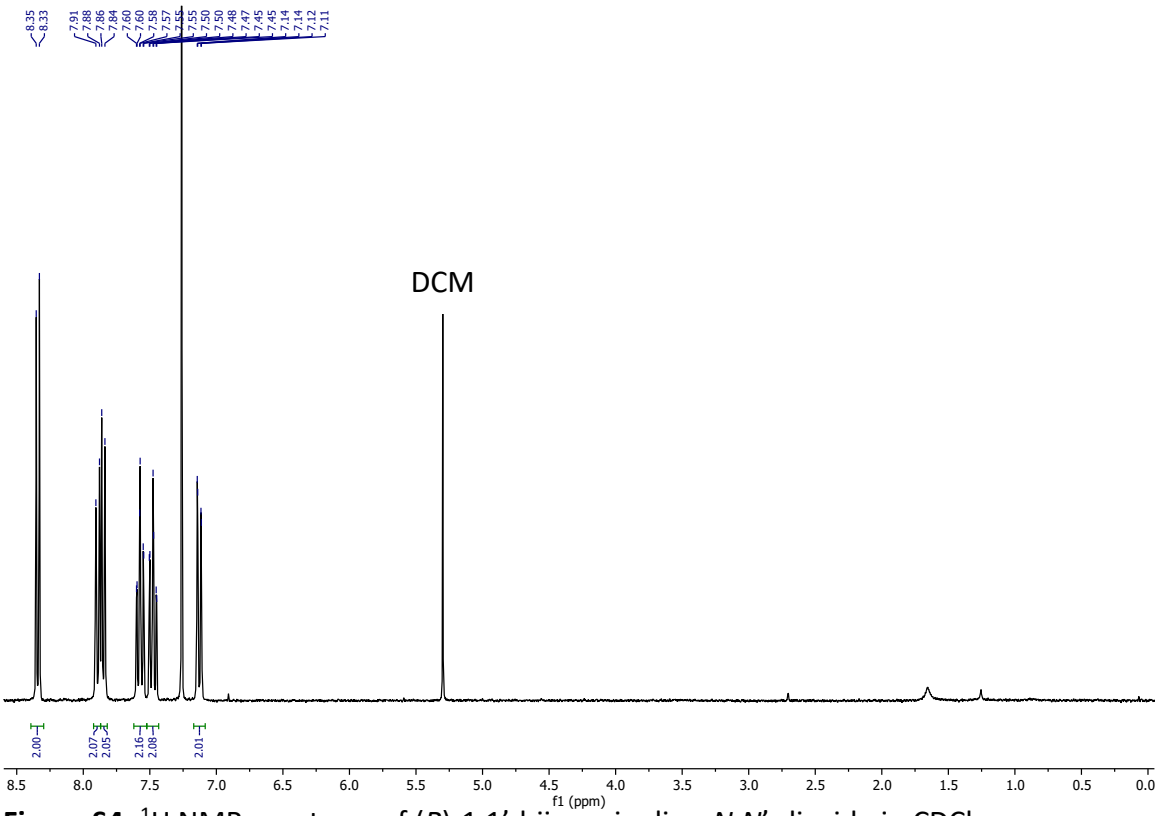

Figure S4: ^{1}H NMR spectrum of (*R*)-1,1'-biisoquinoline-*N*,*N*'-dioxide in $CDCl_3$

Synthesis of Lanthanide Complexes

Synthesis of $[(R\text{-BIQNO})_4Yb][OTf]_3$

To a stirred solution of (*R*)-biisoquinoline dioxide (50 mg, 0.17 mmol, 4 equiv) in 10 mL of anhydrous THF, a solution of $Yb(OTf)_3$ (27 mg, 0.04 mmol, 1 equiv) in 5 mL of anhydrous THF was added dropwise, and the reaction mixture was stirred for three days at room temperature. THF was pumped off under high vacuum to obtain a white solid, which was washed with cold, dry THF and then dried under high vacuum.

^{1}H NMR (300 MHz, CD_3CN) δ 12.71 (d, *J* = 8.1 Hz), 10.28 (t, *J* = 7.4 Hz), 10.01 (t, *J* = 7.6 Hz), 9.95 (d, *J* = 8.4 Hz), 6.63 (s), -22.13 (s).

^{19}F NMR (376 MHz, CD_3CN) δ -79.84.

^{13}C NMR (101 MHz, CD_3CN) δ 168.0, 140.9, 139.1, 136.4, 135.9, 132.7, 132.4, 128.2.

Molecular formula of the complex: $C_{75}H_{48}F_9N_8O_{17}S_3Yb$. Elemental Analysis: Calcd (%): C, 50.79; H, 2.73; N, 6.32. Found (%): C, 50.74; H, 2.72; N, 6.28.

Synthesis of [(*R*-BIQNO)$_4$Er][OTf]$_3$

The complex was synthesized using the same experimental procedure outlined above using Er(OTf)$_3$.

^{1}H NMR (300 MHz, CD_3CN) δ 19.34 (s), 13.10 (s), 12.91 (s), 11.70 (s), 7.37 (s), -59.64 (s).

^{19}F NMR (376 MHz, CD_3CN) δ -81.35.

^{13}C NMR (101 MHz, CD_3CN) δ 200.6, 160.4, 142.5, 140.9, 139.3, 137.1, 136.3, 132.2.

Molecular formula of the complex: $C_{75}H_{48}F_9N_8O_{17}S_3Er$. Elemental Analysis: Calcd (%): C, 50.96; H, 2.74; N, 6.34. Found (%): C, 51.09; H, 2.85; N, 6.29.

Synthesis of [(*R*-BIQNO)$_4$Y][OTf]$_3$

The complex was synthesized using the same experimental procedure outlined above using Y(OTf)$_3$.

^{1}H NMR (300 MHz, CD_3CN) δ 8.88 (dd, *J* = 7.2, 1.6 Hz, 2H), 7.84 (d, *J* = 7.1 Hz, 2H), 7.78 – 7.70 (m, 4H), 7.50 (ddd, *J* = 8.4, 5.0, 3.3 Hz, 2H), 6.93 (d, *J* = 8.6 Hz, 2H).

^{19}F NMR (376 MHz, CD_3CN) δ -79.29.

^{13}C NMR (101 MHz, CD_3CN) δ 137.7, 137.7, 132.2, 131.9, 130.9, 128.0, 127.6, 125.6, 125.3.

Molecular formula of the complex: $C_{75}H_{48}F_9N_8O_{17}S_3Y$. Elemental Analysis: Calcd (%): C, 53.32; H, 2.86; N, 6.63. Found (%): C, 53.22; H, 2.92; N, 6.63.

Synthesis of [(*S*-BIQNO)$_4$Yb][OTf]$_3$

To a stirred solution of (*S*)-biisoquinoline dioxide (50 mg, 0.17 mmol, 4 equiv) in 10 mL of anhydrous THF, a solution of Yb(OTf)$_3$ (27 mg, 0.04 mmol, 1 equiv) in 5 mL of anhydrous THF was added dropwise, and the reaction mixture was stirred for three days at room temperature. THF was pumped off under high vacuum to obtain a white solid, which was washed with cold, dry THF and then dried under high vacuum.

^{1}H NMR (300 MHz, CD_3CN) δ 12.73 (d, *J* = 8.2 Hz), 10.29 (t, *J* = 7.4 Hz), 10.02 (t, *J* = 7.6 Hz), 9.95 (d, *J* = 8.4 Hz), 6.62 (s), -22.29 (s).

^{19}F NMR (376 MHz, CD_3CN) δ -80.02.

^{13}C NMR (101 MHz, CD_3CN) δ 168.0, 140.9, 139.1, 136.4, 135.9, 132.7, 132.5, 128.2.

Molecular formula of the complex: $C_{75}H_{48}F_9N_8O_{17}S_3Yb$. Elemental Analysis: Calcd (%): C, 50.79; H, 2.73; N, 6.32. Found (%): C, 50.79; H, 2.71; N, 6.28.

Synthesis of [(*S*-BIQNO)$_4$Er][OTf]$_3$

The complex was synthesized using the same experimental procedure outlined above using Er(OTf)$_3$.

^{1}H NMR (300 MHz, CD_3CN) δ 19.35 (s), 13.11 (s), 12.91 (s), 11.71 (s), 7.37 (s), -60.00 (s).

^{19}F NMR (376 MHz, CD_3CN) δ -80.42.

^{13}C NMR (101 MHz, CD_3CN) δ 160.1, 142.2, 140.6, 139.0, 136.8, 131.9.

Molecular formula of the complex: $C_{75}H_{48}F_9N_8O_{17}S_3Er$. Elemental Analysis: Calcd (%): C, 50.96; H, 2.74; N, 6.34. Found (%): C, 51.12; H, 2.81; N, 6.30.

Complex NMR Spectra

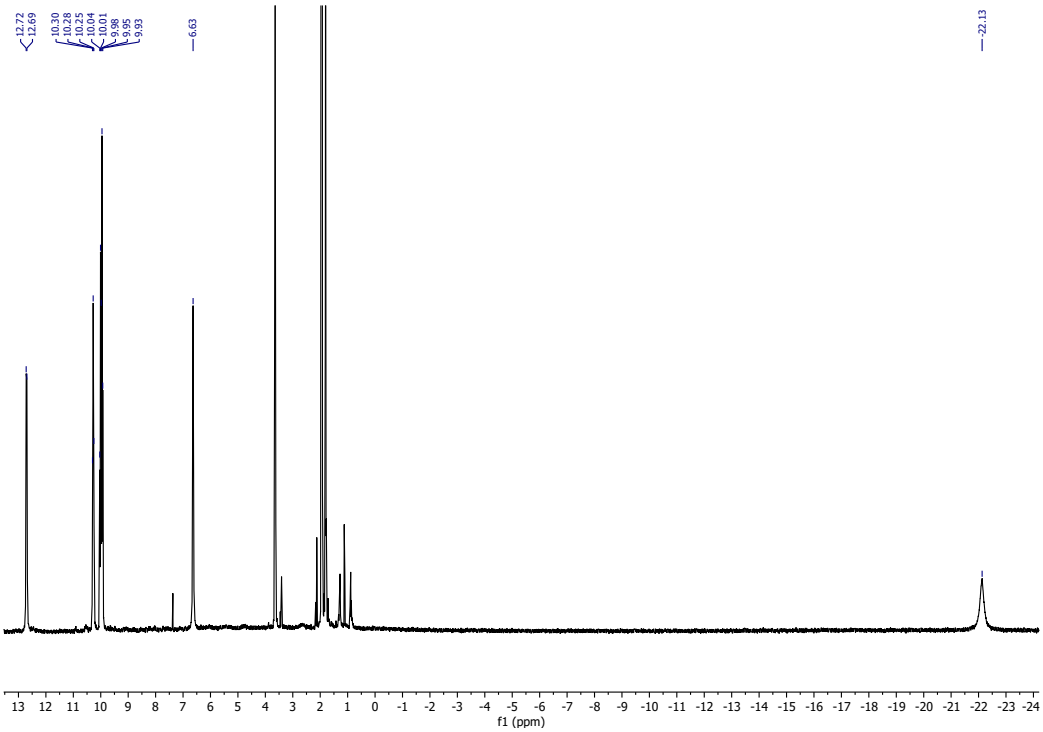

Figure S5: ^{1}H NMR spectrum of [(*R*-BIQNO)$_4$Yb][OTf]$_3$ in d$_3$-acetonitrile

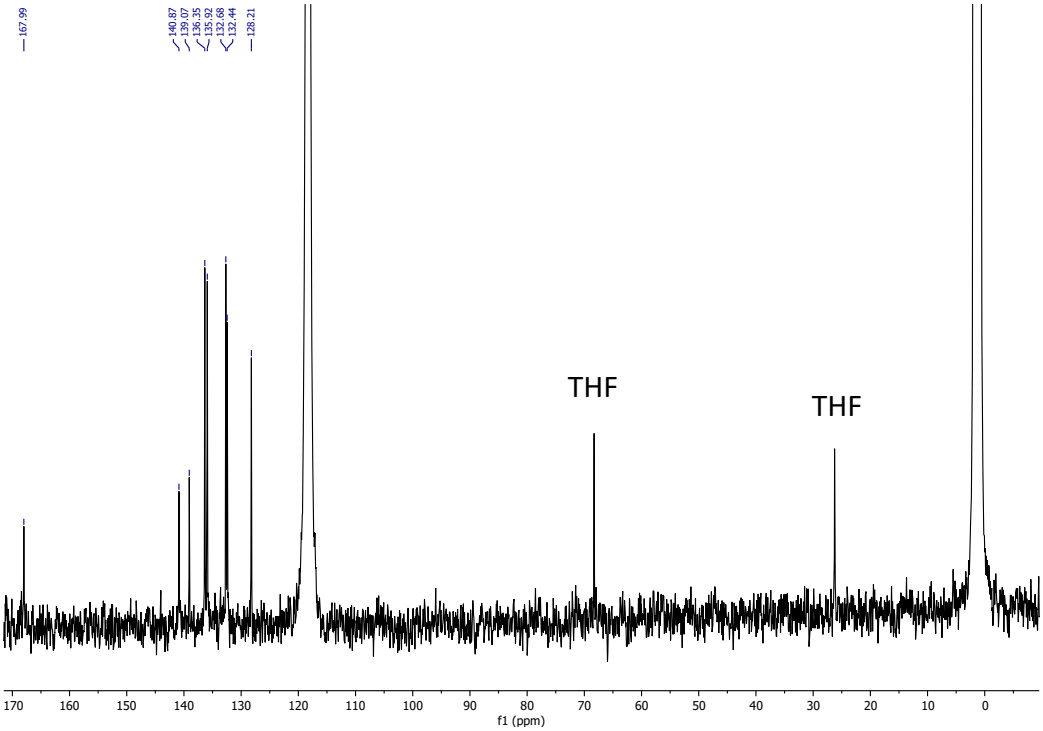

Figure S6: ^{13}C NMR spectrum of [(*R*-BIQNO)$_4$Yb][OTf]$_3$ in d$_3$-acetonitrile

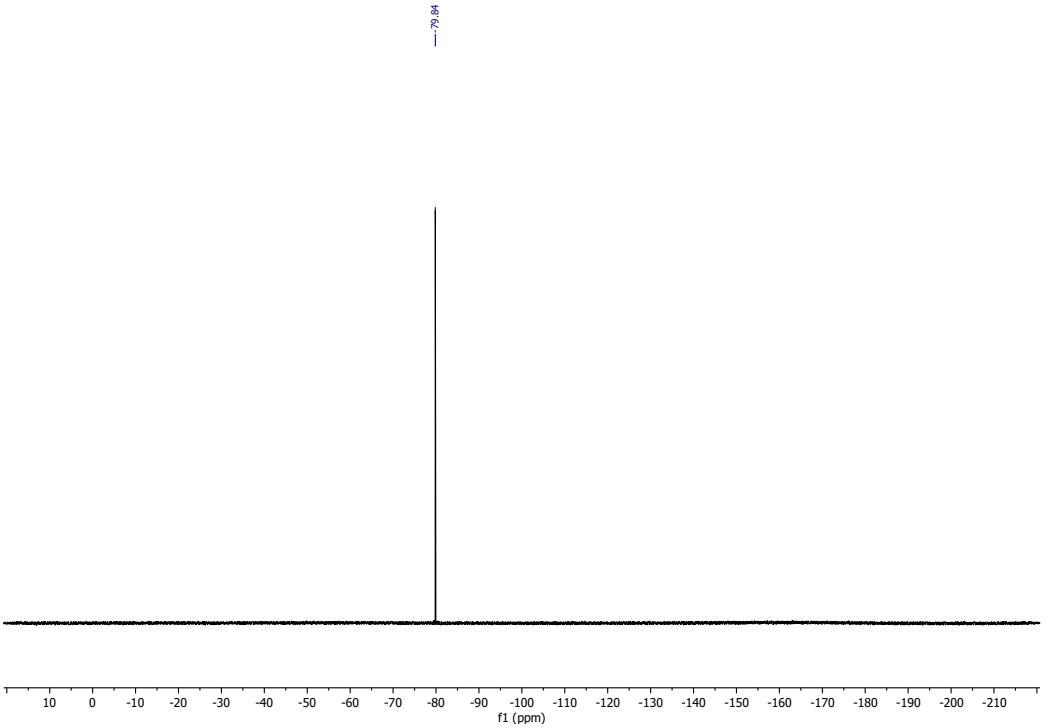

Figure S7: ^{19}F NMR spectrum of [(*R*-BIQNO)$_4$Yb][OTf]$_3$ in d$_3$-acetonitrile

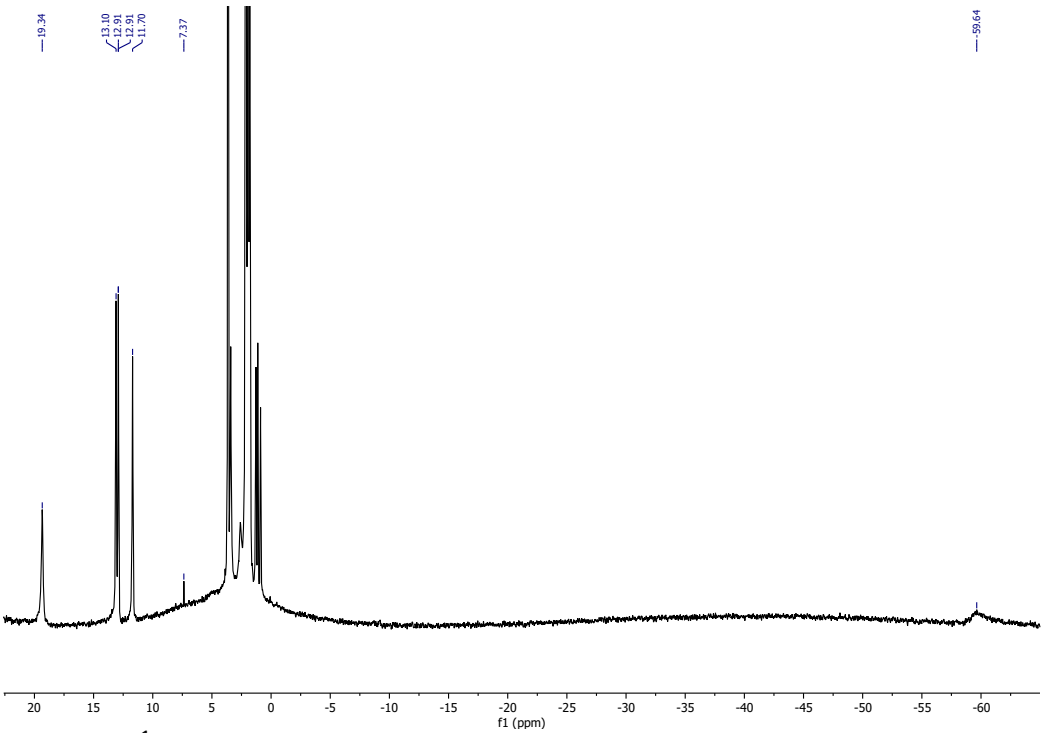

Figure S8: ^{1}H NMR spectrum of [(*R*-BIQNO)$_4$Er][OTf]$_3$ in d$_3$-acetonitrile

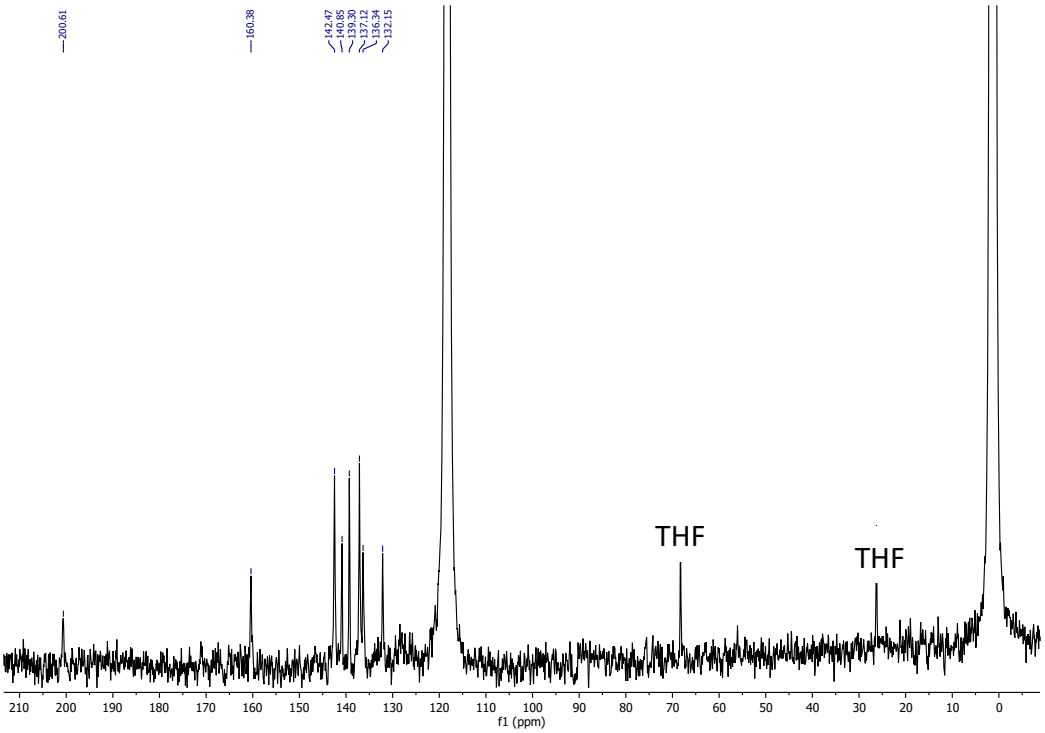

Figure S9: ^{13}C NMR spectrum of [(*R*-BIQNO)$_4$Er][OTf]$_3$ in d$_3$-acetonitrile

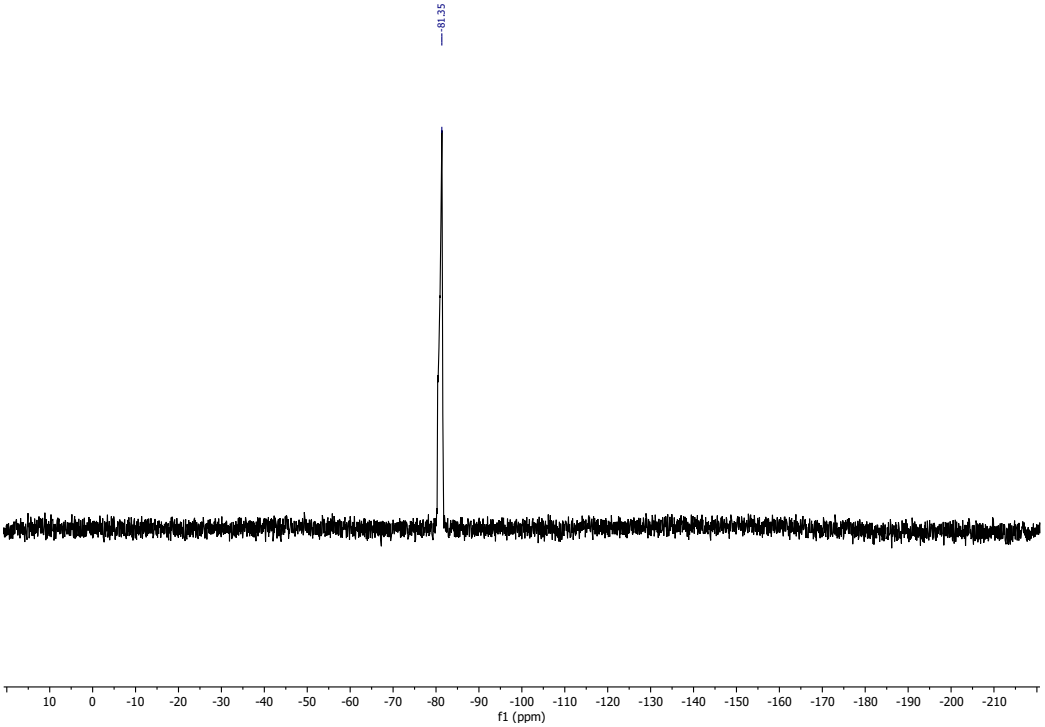

Figure S10: ^{19}F NMR spectrum of [(*R*-BIQNO)$_4$Er][OTf]$_3$ in d$_3$-acetonitrile

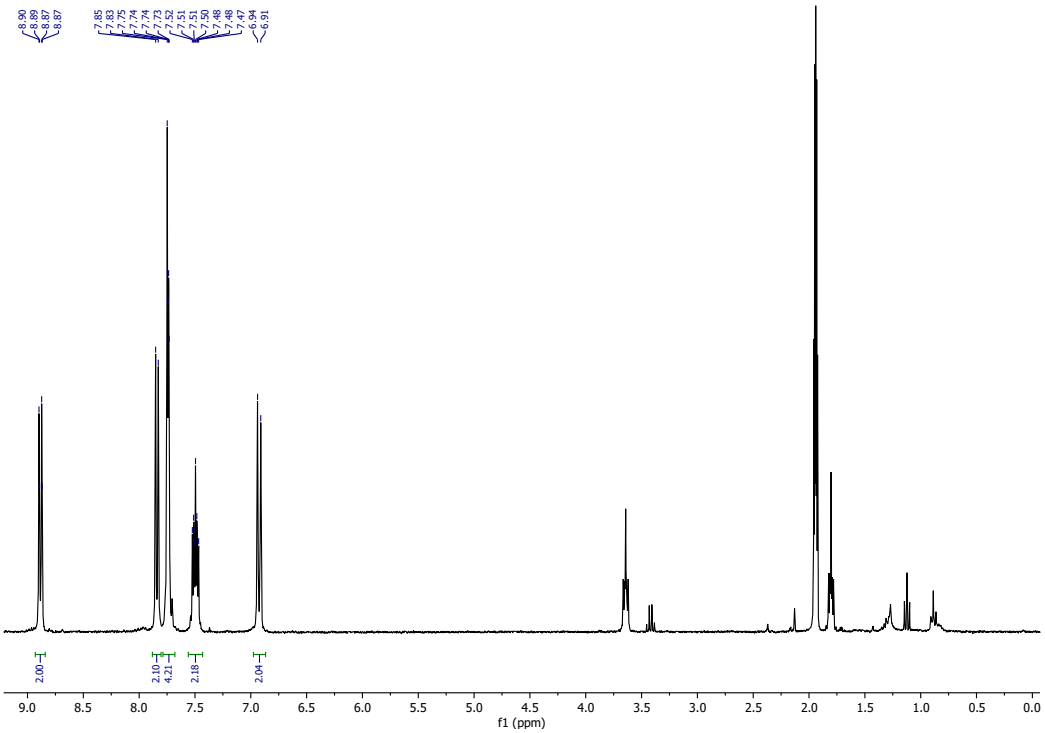

Figure S11: ^{1}H NMR spectrum of [(*R*-BIQNO)$_4$Y][OTf]$_3$ in d$_3$-acetonitrile

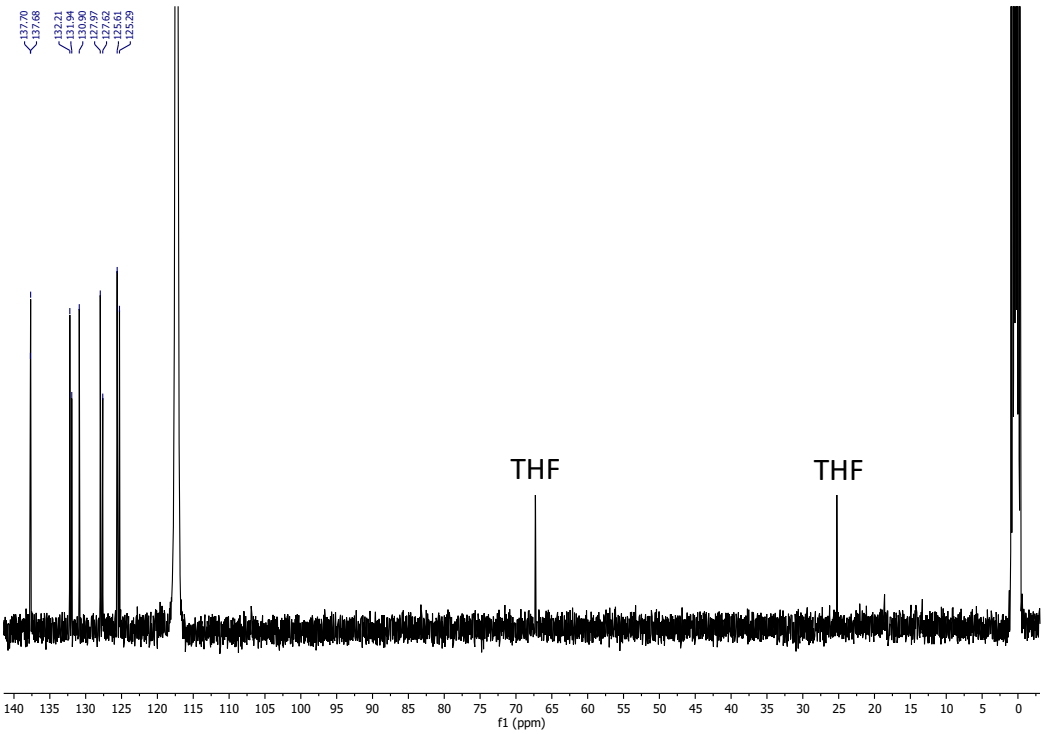

Figure S12: ^{13}C NMR spectrum of [(*R*-BIQNO)$_4$Y][OTf]$_3$ in d$_3$-acetonitrile

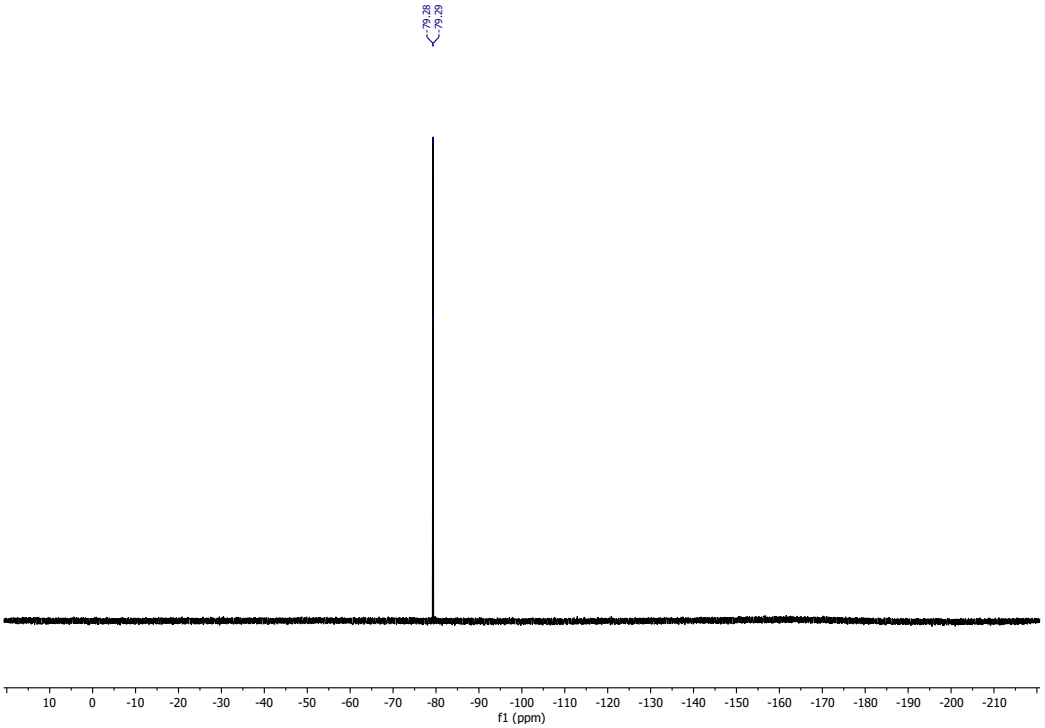

Figure S13: ^{19}F NMR spectrum of [(*R*-BIQNO)$_4$Y][OTf]$_3$ in d$_3$-acetonitrile

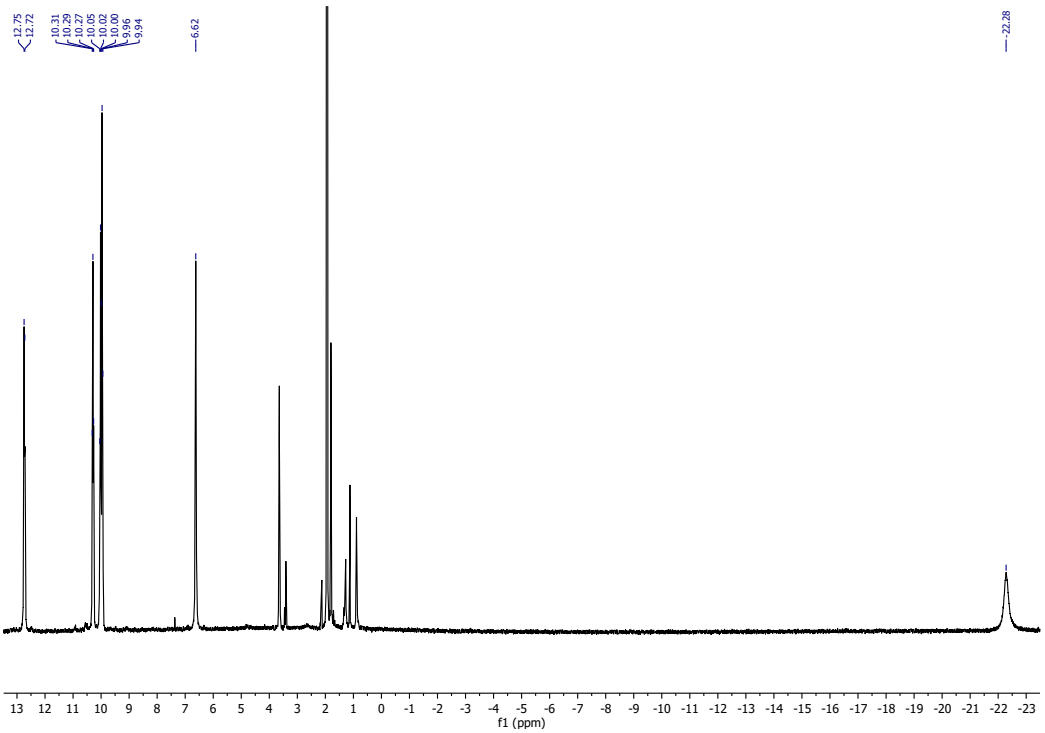

Figure S14: ^{1}H NMR spectrum of [(*S*-BIQNO)$_4$Yb][OTf]$_3$ in d$_3$-acetonitrile

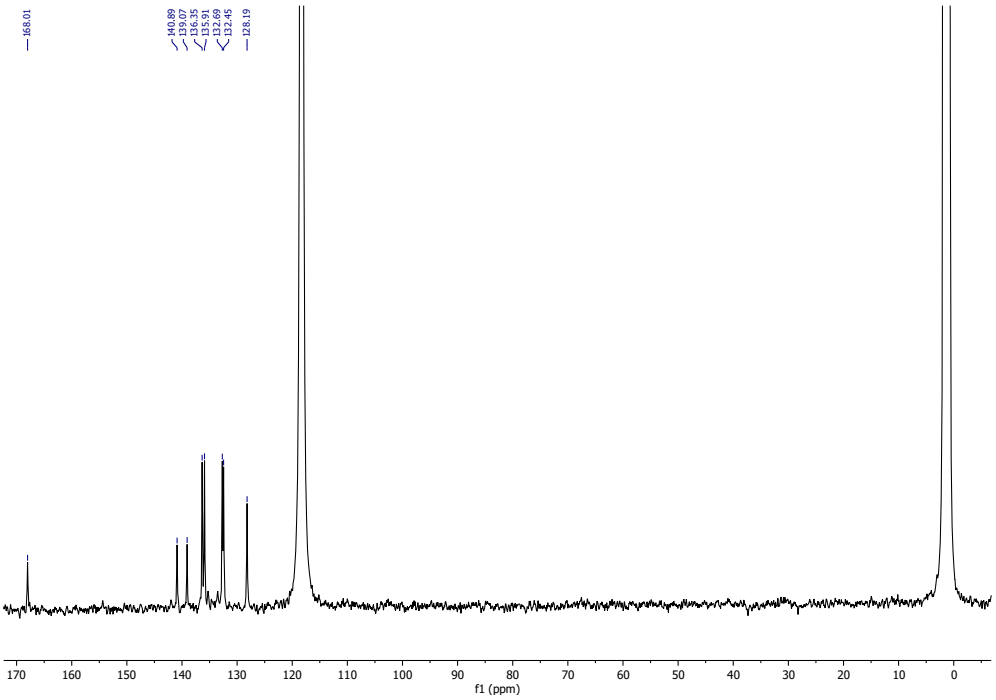

Figure S15: ^{13}C NMR spectrum of [(*S*-BIQNO)$_4$Yb][OTf]$_3$ in d$_3$-acetonitrile

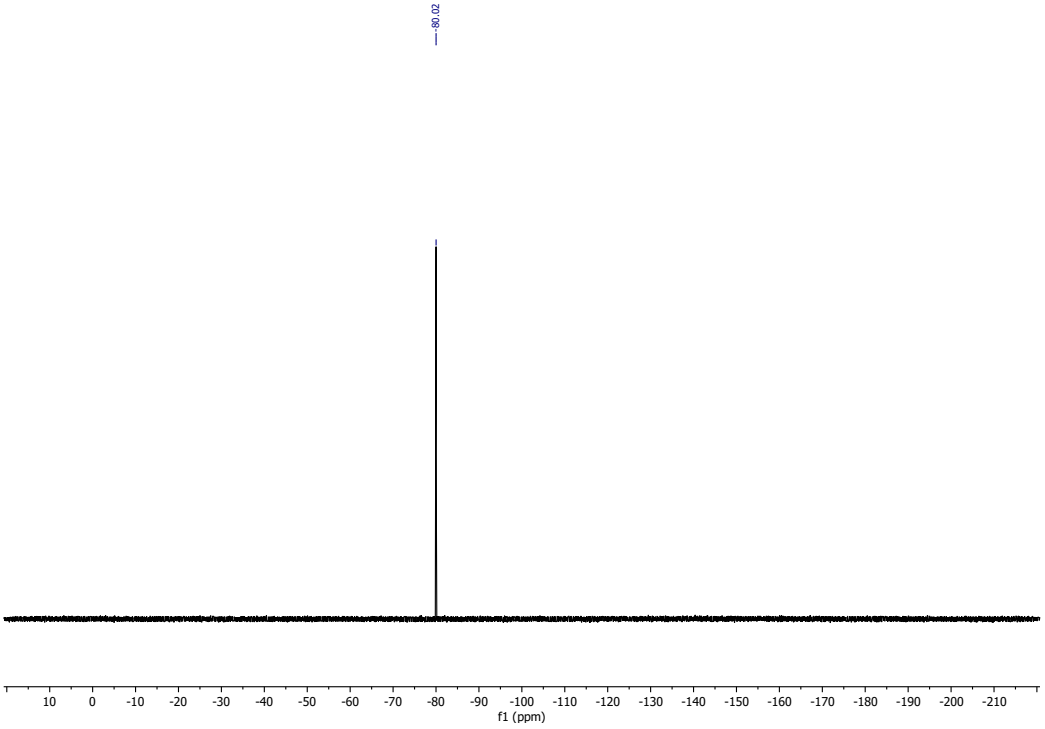

Figure S16: ^{19}F NMR spectrum of [(*S*-BIQNO)$_4$Yb][OTf]$_3$ in d$_3$-acetonitrile

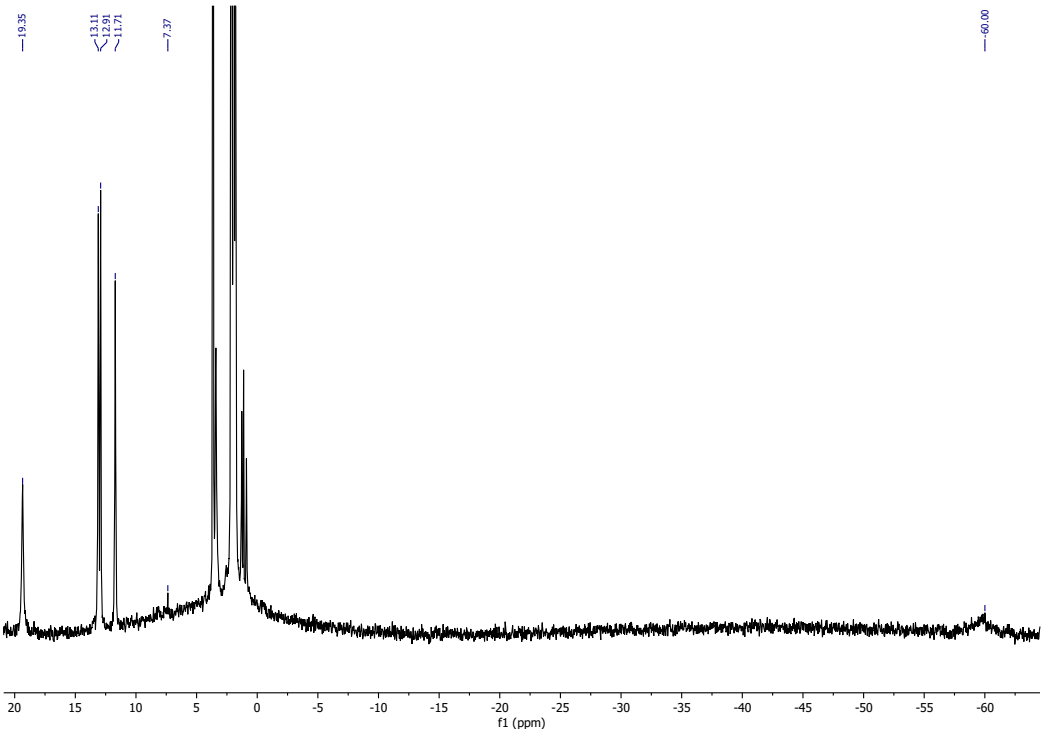

Figure S17: ^{1}H NMR spectrum of [(*S*-BIQNO)$_4$Er][OTf]$_3$ in d$_3$-acetonitrile

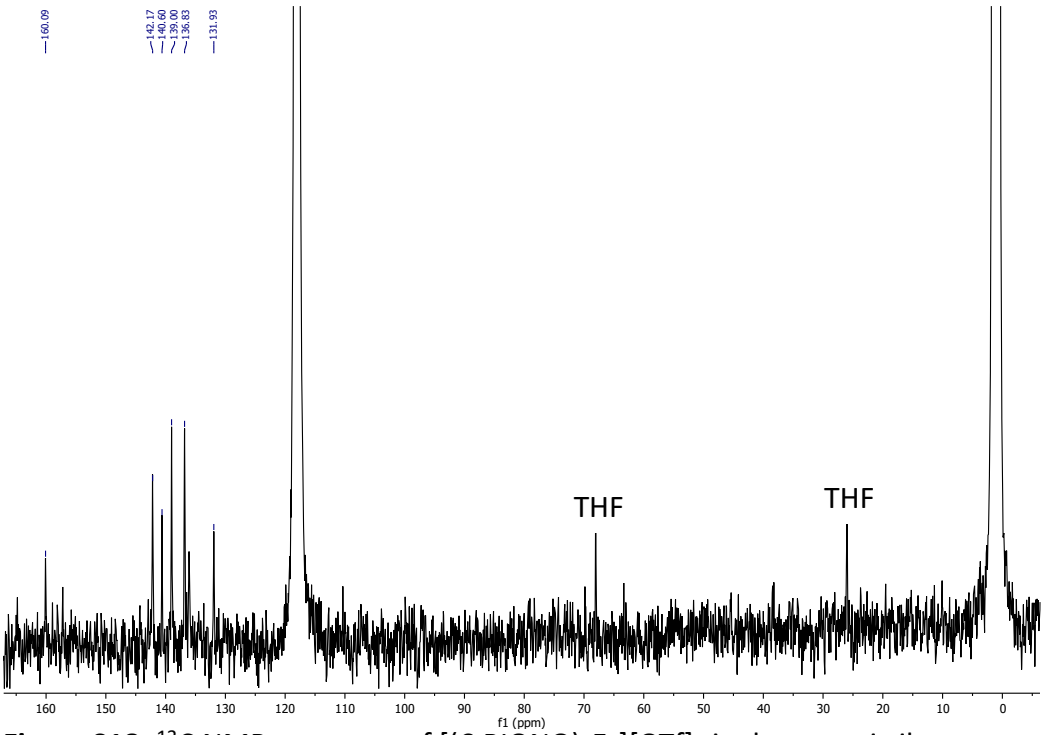

Figure S18: ^{13}C NMR spectrum of [(*S*-BIQNO)$_4$Er][OTf]$_3$ in d$_3$-acetonitrile

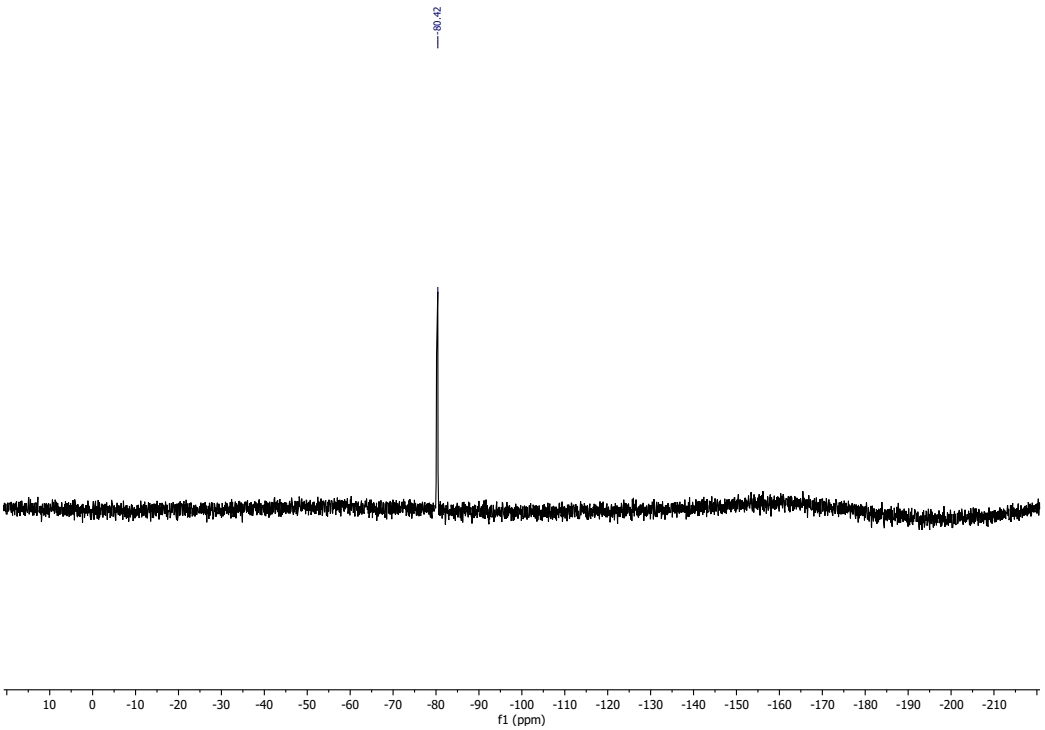

Figure S19: ^{19}F NMR spectrum of $[(S\text{-BIQNO})_4Er][OTf]_3$ in d_3-acetonitrile

Absorption, Emission and Excitation Spectra of the Complexes

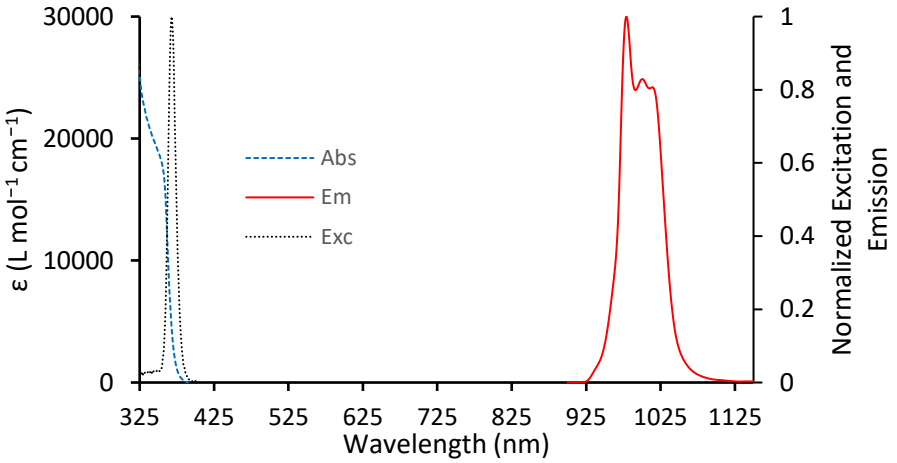

Figure S20: Absorption, Excitation, and Emission Spectra for $[Yb(BIQNO)_4][OTf]_3$

Collected from a 1.6×10^{-4} M solution in 1,2-difluorobenzene at room temperature. Absorption spectrum collected in a 1 cm path length cuvette with a bandpass of 5 nm. The excitation spectrum was collected with excitation/emission bandpass of 5/5 nm with the emission wavelength fixed at 975 nm. Emission spectrum collected with a 365 nm excitation LED with 10 nm bandpass.

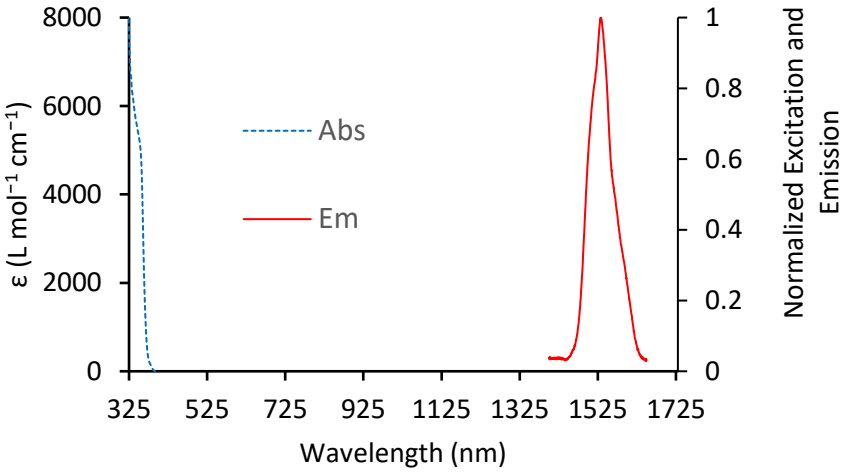

Figure S21: Absorption and Emission Spectra for $[Er(BIQNO)_4][OTf]_3$

Collected from a 5.7×10^{-4} M solution in 1,2-difluorobenzene at room temperature. Absorption spectrum collected in a 1 cm path length cuvette with a bandpass of 5 nm. Emission spectrum collected with a 365 nm excitation LED with 26 nm bandpass.

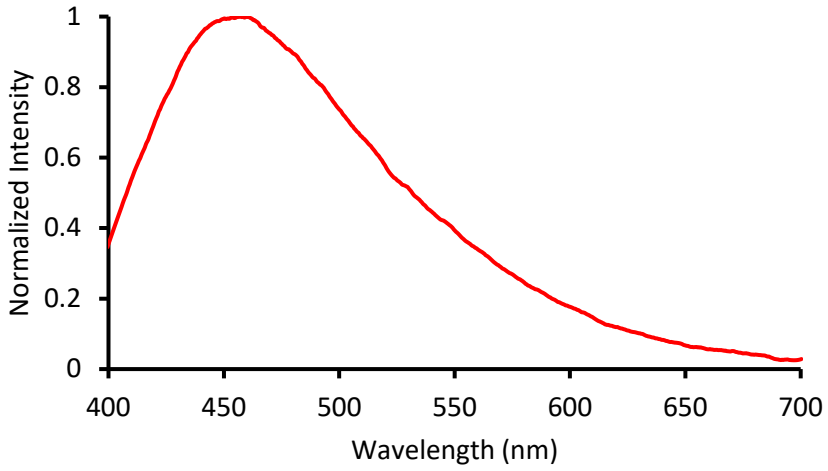

Figure S22: Ligand Singlet Energy for $[Gd(BIQNO)_4][OTf]_3$

Collected from a 5.7×10^{-4} M solution in butyronitrile at room temperature. Emission spectrum collected at 365 nm excitation with excitation/emission bandpass of 10/10 nm. Singlet energy level observed at 455 nm, which corresponds to 21,978 cm^{-1}.

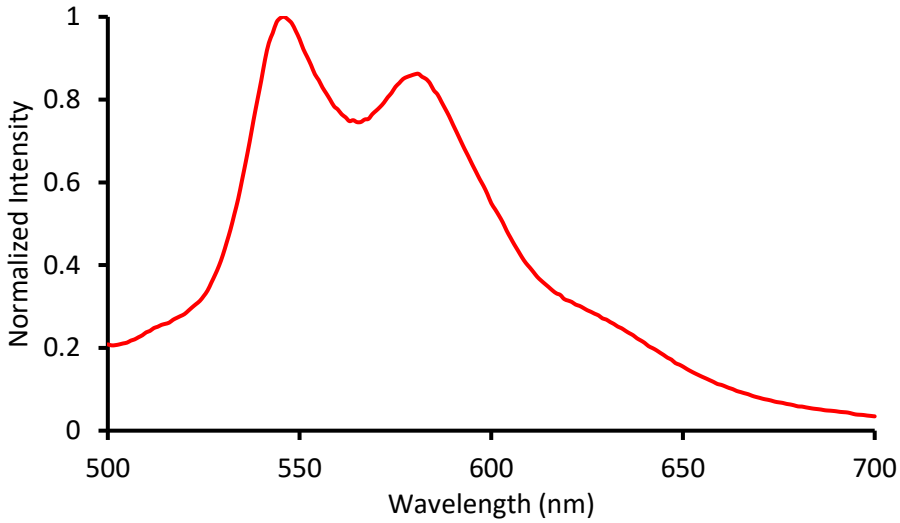

Figure S23: Ligand Phosphorescence for $[Gd(BIQNO)_4][OTf]_3$

Collected from a 5.7×10^{-4} M solution in butyronitrile at 75 K. Emission spectrum collected with 365 nm excitation LED with 2.4 nm bandpass. Triplet energy level observed at 546 nm, which corresponds to 18,315 cm^{-1}.

Lifetime Studies

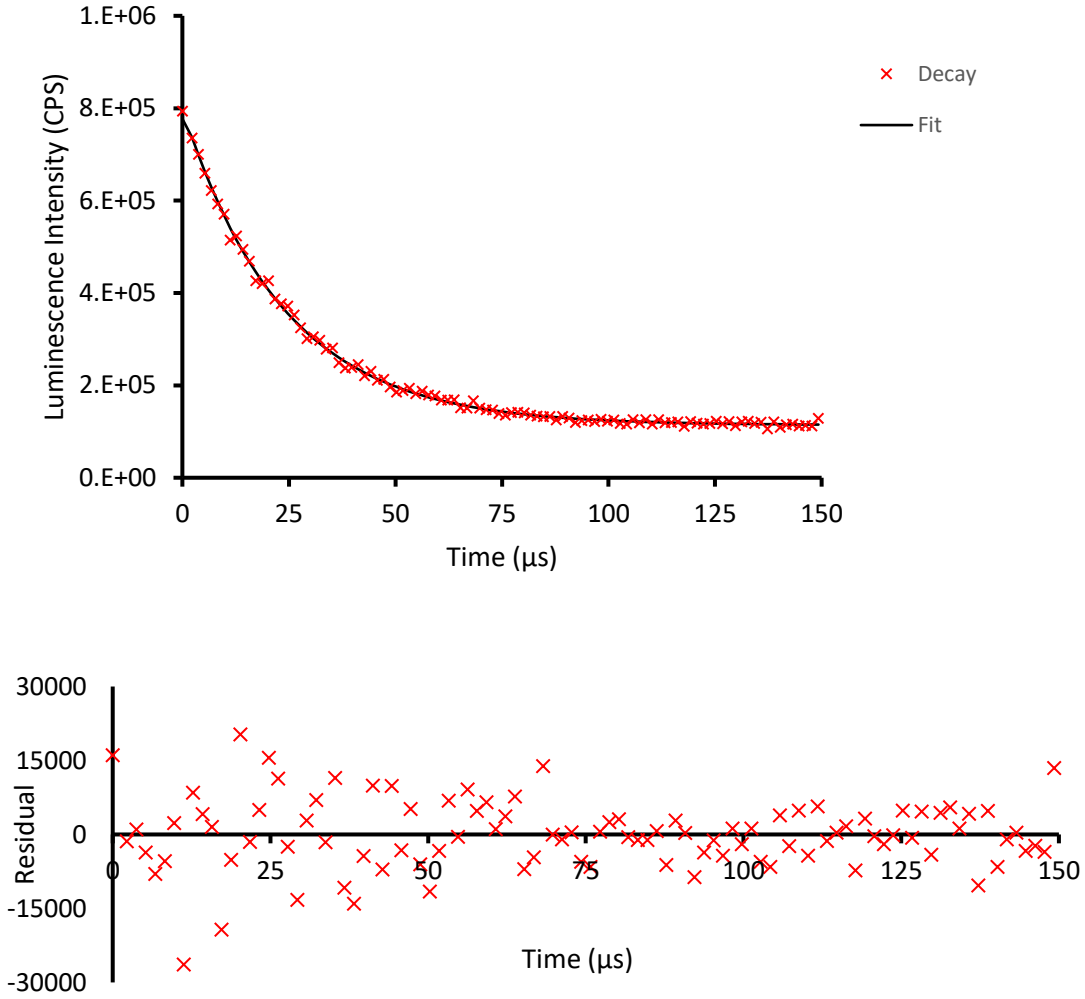

Figure S24: Time-resolved luminescence decay data for $[Yb(BIQNO)_4][OTf]_3$

Collected from a 1.6×10^{-4} M solution in 1,2-difluorobenzene at room temperature after excitation at 380 nm. The observation wavelength was fixed at 983 nm with a fixed bandpass of 26 nm. The plot is an average of 20 runs (τ_{obs} = 35.7 µs).

Due to low emission intensity, luminescence decay for $[Er(BIQNO)_4][OTf]_3$ could not be established.

Circularly Polarized Luminescence Spectra

Solutions of the complexes in 1,2-difluorobenzene were placed in a 3.5 mL quartz cuvette. The sample was illuminated by two 365 nm LEDs positioned opposite each other (0° and 180°) to maximize excitation intensity, resulting in higher signal-to-noise ratio. Luminescence emission was collected at 90° relative to the excitation source at room temperature. Left- and right-circularly polarized emissions were measured sequentially by automatic rotation of the quarter-wave plate between each acquisition. The final spectrum represents the average of twenty consecutive scans.

Regions of low emission intensities in the g_{lum} plots are not reliable, since these are mathematically values that are divided by "0".

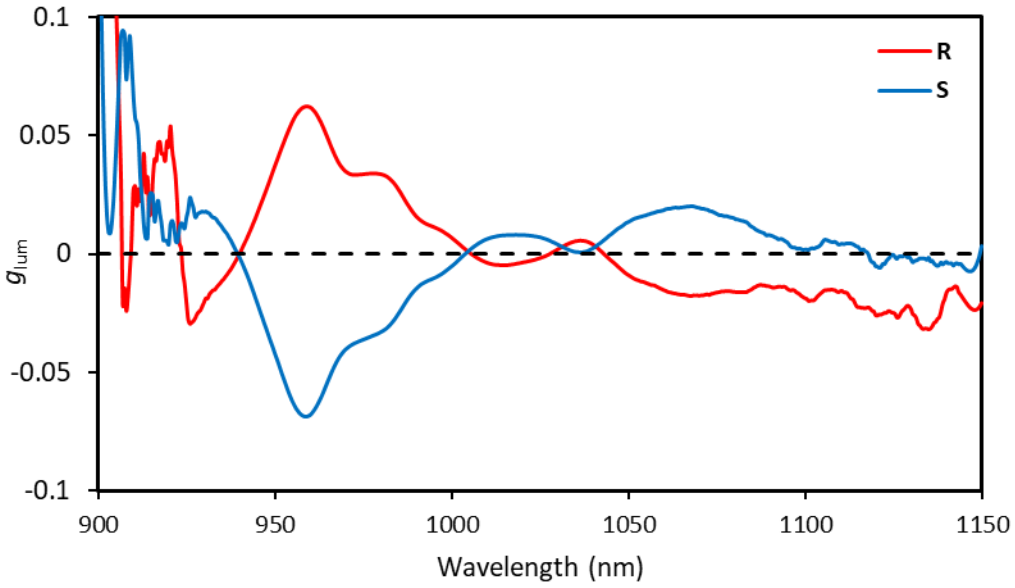

Figure S25: g_{lum} as a function of wavelength for [Yb(*R*/*S*-BIQNO)$_4$][OTf]$_3$

Complexes in 1,2-difluorobenzene at 1.6×10^{-4} M. Excitation at 365 nm, bandpass 10 nm.

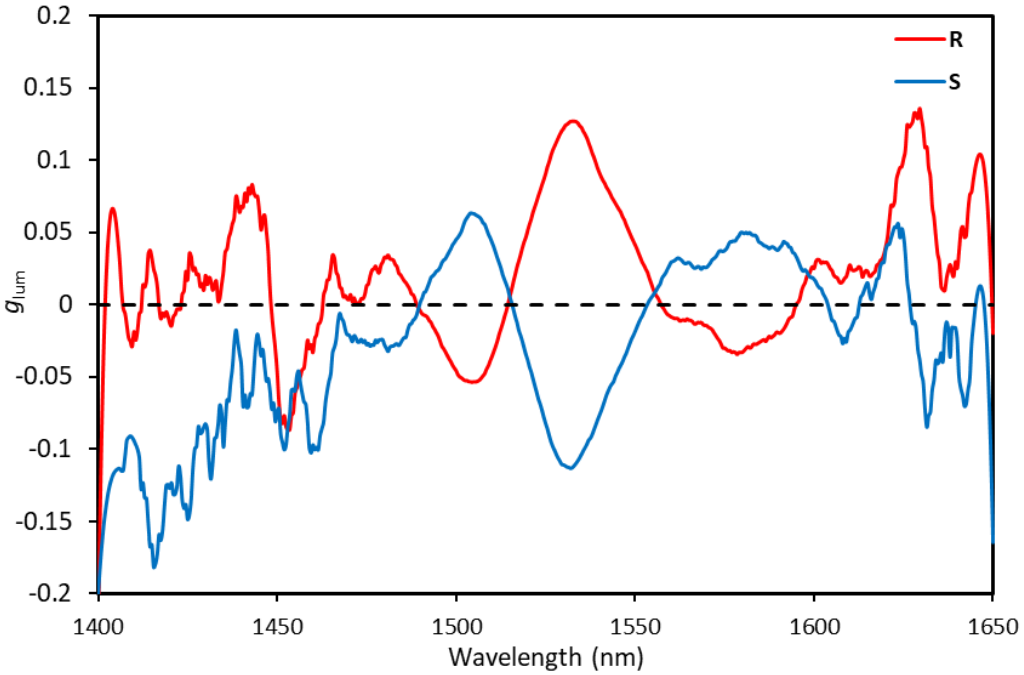

Figure S26: g_{lum} as a function of wavelength for [Er(*R*/*S*-BIQNO)$_4$][OTf]$_3$ Complexes in 1,2-difluorobenzene at 5.7×10^{-4} M. Excitation at 365 nm, bandpass 26 nm.

Quantum Yield Measurements

The luminescence quantum yield of $[Yb(BIQNO)_4][OTf]_3$ was determined in acetonitrile using $[(binol)_3YbNa_3(thf)_6]$ (φ_f = 0.17 in THF) as the reference standard. $[Yb(BIQNO)_4][OTf]_3$ complex was subsequently employed as the standard for $[Er(BIQNO)_4][OTf]_3$. Quantum yields were calculated according to the equation:

$$\phi \text{ sample} = \phi \text{ standard} \times \frac{m\ sample}{m\ standard} \times \left(\frac{\eta\ sample}{\eta\ standard}\right)^2$$

Where ϕ is the quantum yield, m is the slope obtained from the plot of integrated emission intensity versus absorbance, and η represents the refractive index of the solvent.

CPL Brightness

Table S1: Tabulated B_{CPL} data

Complex	λ (nm)	ε ($M^{-1}cm^{-1}$) at 365 nm	ϕ	Transition	$\lvert g_{lum}\rvert$	β_i	B_{CPL} ($M^{-1}cm^{-1}$)	$^{Ln}B_{CPL}$ ($M^{-1}cm^{-1}$)	Lifetime (μs)
$[Er(BIQNO)_4][OTf]_3$	1533	1689	0.0306	$^4I_{13/2} \rightarrow {}^4I_{15/2}$	0.12	1	3.1	1.3	
$[Yb(BIQNO)_4][OTf]_3$	979	7474	0.0616	$^4F_{5/2} \rightarrow {}^4F_{7/2}$	0.07	1	16.1	12.6	35.7

B_{CPL} values were calculated using the equation: $B_{CPL} = \frac{1}{2} \times \varepsilon \times \phi \times \beta_i \times |g_{lum}|$

The excitation wavelength used was 380 nm.

An adjusted expression of B_{CPL}, specific to lanthanides (and possibly actinides), was used as follows[10,11]:

$$^{Ln/An}B_{CPL}(\lambda_x) = \varepsilon \times \phi \times \beta_i \times \frac{|\int \Delta I_i d\lambda_i|}{\int |\Delta I_i| d\lambda_i} \times \frac{|g_{lum}(\lambda_x)|}{2}$$

Where:

ε − Molar absorptivity

ϕ − Quantum yield

β_i – Branching ratio for the transition

$d\lambda_i$ – The range of wavelength for the transition i

$\frac{|\int \Delta I_i d\lambda_i|}{\int |\Delta I_i| d\lambda_i}$ – The ratio of positive/negative contributions of the ΔI over the transition i

$g_{lum}(\lambda_X)$ – Maximum dissymmetry factor corresponding to the sign of $\frac{|\int \Delta I_i d\lambda_i|}{\int |\Delta I_i| d\lambda_i}$ within the transition i, measured at the specific wavelength λ_X.

Circular Dichroism Spectra

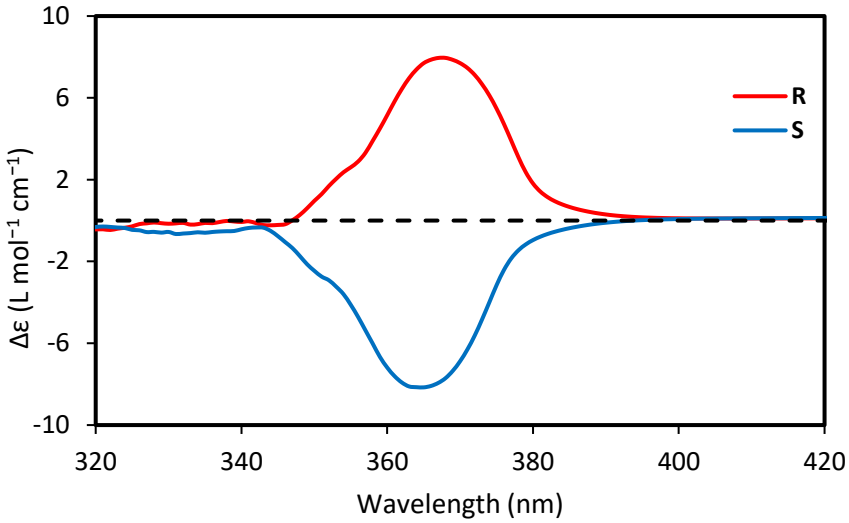

Figure S27: Circular dichroism as a function of wavelength for [Yb(*R*/*S*-BIQNO)$_4$][OTf]$_3$ Complexes in acetonitrile at 5.64 × 10^{-4} M.

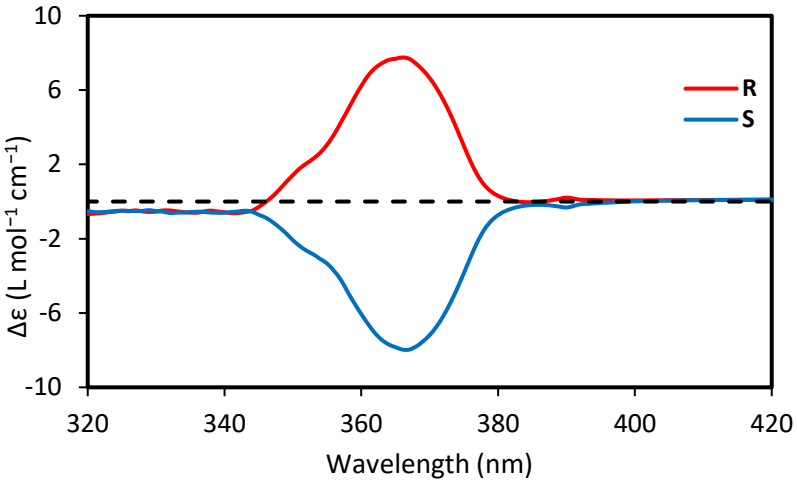

Figure S28: Circular dichroism as a function of wavelength for [Er(*R*/*S*-BIQNO)$_4$][OTf]$_3$ Complexes in acetonitrile at 5.66 × 10^{-4} M.

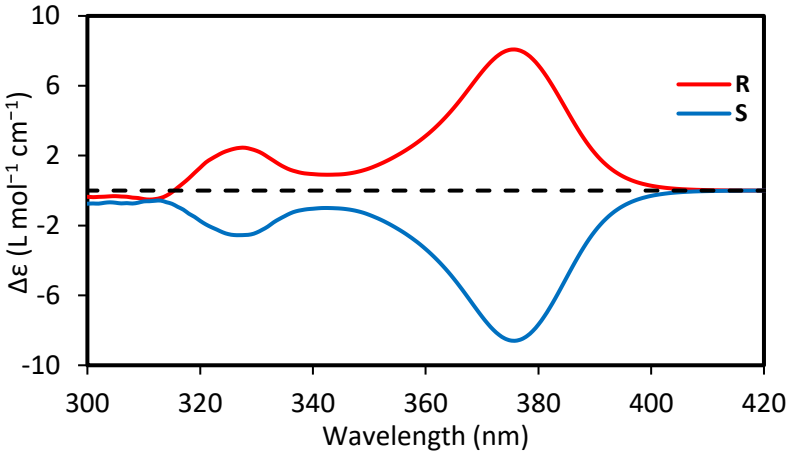

Figure S29: Circular dichroism as a function of wavelength for (*R*/*S*-BIQNO) Enantiomers in acetonitrile at 6.94×10^{-4} M.

X-ray Crystallography

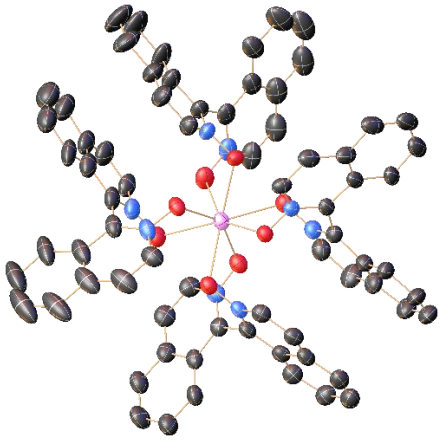

Figure S30: SC-XRD structure for [Er(*S*-BIQNO)$_4$][OTf]$_3$

Table S2: Crystal data and structure refinement for [Er(*S*-BIQNO)$_4$][OTf]$_3$.

Identification code	[Er(*S*-BIQNO)$_4$][OTf]$_3$
Empirical formula	$C_{72}H_{48}N_8O_8Er$
Formula weight	1320.48
Temperature/K	293(2)
Crystal system	orthorhombic
Space group	$P2_12_12_1$
a/Å	14.086(3)
b/Å	25.727(6)
c/Å	44.479(9)
α/°	90
β/°	90
γ/°	90
Volume/Å^3	16119(6)
Z	8
ρ_{calc}g/cm^3	1.452
μ/mm^{-1}	1.209
F(000)	7076.0
Crystal size/mm^3	0.103 × 0.099 × 0.021
Radiation	Mo Kα (λ = 0.71073)
2Θ range for data collection/°	3.772 to 56.628
Index ranges	-18 ≤ h ≤ 18, -34 ≤ k ≤ 34, -59 ≤ l ≤ 59
Reflections collected	514195
Independent reflections	39993 [R_{int} = 0.0559, R_{sigma} = 0.0307]
Data/restraints/parameters	39993/25290/2026
Goodness-of-fit on F^2	1.052
Final R indexes [I>=2σ (I)]	R_1 = 0.0869, wR_2 = 0.2452
Final R indexes [all data]	R_1 = 0.1007, wR_2 = 0.2666
Largest diff. peak/hole / e Å^{-3}	2.88/-2.54
Flack parameter	0.034(2)

Table S3. Summarized optical and chiroptical data for reported NIR-CPL complexes.

Complex	**Symmetry**	**ε (M^{-1} cm^{-1})**	**Φ (%)**	**τ (μs)**	**g_{lum}‡ at (nm)**	**B_{CPL} (M^{-1} cm^{-1})**	**$^{Ln}B_{CPL}$ (M^{-1} cm^{-1})**
$[Yb(Binol)_3][Na]_3$[12]	D_3	26000	17	—	±0.17 (975)	379	160
$Yb(Binol)_3][TMGH]_3$[13]	D_3	—	—	—	±0.066 (954)	—	—
$[Yb(Vanol)_3][Na]_3$[14]	D_3	11500	10.1	32.2	±0.21 (975)	122.3	38.8
$[Yb(Sphenol)_3][Na]_3$[15]	D_3	17820	7.5	11.6	±0.22 (973)	146.3	66.0
$[Yb(F_2\text{-}Binol)_3][TMGH]_3$[16]	D_3	20600	1.8	2.7	±0.125 (963)	23.2	—
$[Yb(hfbc)_4][Cs]$[13]	C_4	—	—	—	±0.38 (988)	—	—
$[Yb(^{i}PrPyBox)(TTA)_3]$[17]	C_1	52000	0.69	—	±0.029 (972)	5.2	—
$[Yb(PhPyBox)(TTA)_3]$[17]	C_1	42000	0.62	—	±0.019 (970)	2.5	—
$[Yb(pydac)(Binol)_2][Na]$[18]	C_2	27000	—	2.49 2.06	±0.01 (980)	—	—
$[Yb_2(BTHP)_4]$[19]	D_4*	—	6.5	14	±0.81 (980)	821	—
$[Yb(BIQNO)_4][OTf]_3$	D_2	7474	6.2	35.7	±0.07 (959)	16.1	12.6
$[Er(Binol)_3][Na]_3$[12]	D_3	42000	0.58	—	±0.47 (1540)	57.3	22.1
$[Er(Binol)_3][TMGH]_3$[13]	D_3	59279	0.0002	0.4	±0.29 (1545)	0.017	—
$[Er(Vanol)_3][Na]_3$[14]	D_3	12900	0.48	3.91	±0.64 (1540)	19.5	11.5
$[Er(Sphenol)_3][Na]_3$[15]	D_3	19060	0.28	2.8	±0.77 (1540)	20.7	16.5
$[Er(F_{12}\text{-}Binol)_3][Li]_3$[20]	D_3	24000	11	34	±0.24 (1530)	317	23.6
$[Er(F_{12}\text{-}Binol)_3][K]_3$[20]	D_3	62000	3.5	10	±0.17 (1526)	184	33.8
$[Er(hfbc)_4][Cs]$[21]	C_4	34830	0.07	6.6	+0.83 (1510)	0.23	—
$[Er(pybam)_3][OTf]_3$[22]	D_3	102000	—	0.21	±0.66 (1519)	—	—
$[Er(pybox)_2][OTf]_3$[23]	C_2	60000	0.04	4	±0.33 (1539)	0.7	—
$[Er(BIQNO)_4][OTf]_3$	D_2	1689	3.1	—	±0.12 (1535)	3.1	1.3

‡values reported in the literature, head-to-head comparisons may not be perfectly accurate due to bandpass differences *C_4 at metal.

References

1. W.-W. Xie, Y. Liu, R. Yuan, D. Zhao, T.-Z. Yu, J. Zhang, C.-S. Da, Transition metal-free homocoupling of unactivated electron-deficient azaarenes, *Adv. Synth. Catal.*, 2016, **358**, 994–1002.
2. C. Reep, P. Morgante, R. Peverati, N. Takenaka, Axial-chiral biisoquinoline *N*,*N*'-dioxides bearing polar aromatic C-H bonds as catalysts in Sakurai-Hosomi-Denmark allylation, *Org. Lett.*, 2018, **20**, 5757–5761.
3. M. Nakajima, M. Saito, M. Shiro, S. I. Hashimoto, (S)-3,3'-dimethyl-2,2'-biquinoline *N*,*N*'-dioxide as an efficient catalyst for enantioselective addition of allyltrichlorosilanes to aldehydes, *J. Am. Chem. Soc.*, 1998, **120**, 6419–6420.
4. Bruker AXS SE, SAINT, version 8.42, 2025.
5. L. Krause, R. Herbst-Irmer, G. M. Sheldrick, D. Stalke, Comparison of silver and molybdenum microfocus X-ray sources for single-crystal structure determination, *J. Appl. Crystallogr.*, 2015, **48**, 3–10.
6. G. M. Sheldrick, SHELXT – integrated space-group and crystal-structure determination, *Acta Cryst., Sect. A*, 2015, **71**, 3–8.
7. G. M. Sheldrick, Crystal structure refinement with SHELXL, *Acta Cryst., Sect. C*, 2015, **71**, 3–8.
8. C. R. Groom, I. J. Bruno, M. P. Lightfoot, S. C. Ward, The cambridge structural database, *Acta Cryst., Sect. B, 2016*, **72**, 171–179.
9. D. Kratzert, FinalCif, https://dkratzert.de/finalcif.html, (accessed 3 November 2025).
10. B. A. N. Willis, D. Schnable, N. D. Schley, G. Ung, Spinolate lanthanide complexes for high circularly polarized luminescence metrics in the visible and near-infrared, *J. Am. Chem. Soc.*, 2022, **144**, 22421–22425.
11. O. G. Willis, F. Zinna, L. Di Bari, NIR-circularly polarized luminescence from chiral complexes of lanthanides and d-metals, *Angew. Chem. Int. Ed.*, 2023, **62**, e202302358.
12. N. F. Mukthar, N. D. Schley, G. Ung, Strong circularly polarized luminescence at 1550 nm from enantiopure molecular erbium complexes, *J. Am. Chem. Soc.*, 2022, **144**, 6148–6153.
13. O. G. Willis, F. Zinna, G. Pescitelli, C. Micheletti, L. Di Bari, Remarkable near-infrared chiroptical properties of chiral Yb, Tm and Er complexes, *Dalton Trans.*, 2022, **51**, 518–523.
14. J. A. Adewuyi, N. D. Schley, G. Ung, Vanol-supported lanthanide complexes for strong circularly polarized luminescence at 1550 nm, *Chem. Eur. J.*, 2023, **29**, e202300800.
15. D. Schnable, G. Ung, *Inorg. Chem.*, 2024, **63**, 7378–7385.
16. T. Feng, R. Cai, Z. Zhu, Q. Zhou, A. Sickinger, O. Maury, Y. Guyot, A. Bensalah-Ledoux, S. Guy, B. Baguenard, B. Le Guennic, J. Tang, Enhanced near-infrared circularly polarized luminescence activity in fluorinated binolate ytterbium complexes, *Chem. Eur. J.*, 2025, **31**, e202500910.

17. F. Zinna, L. Arrico and L. Di Bari, Near-infrared circularly polarized luminescence from chiral Yb(III)-diketonates, *Chem. Commun.*, 2019, **55**, 6607–6609.
18. S. Ruggieri, O. G. Willis, S. Mizzoni, E. Cavalli, M. Sanadar, A. Melchior, F. Zinna, L. Di Bari, G. D. Bisag, M. Fochi, L. Bernardi, F. Piccinelli, Near infrared-circularly polarized luminescence/circular dichroism active Yb(III) complexes bearing both central and axial chirality, *Inorg. Chem.*, 2025, **64**, 5505-5512.
19. L. Wang, Z. Yao, W. Huang, T. Gao, P. Yan, Y. Zhou, H. Li, Remarkable 980 nm circularly polarized luminescence from dinuclear Yb(III) helicates with a D4 symmetry, *Inorg. Chem. Front.*, 2023, **10**, 3664–3674.
20. J. A. Adewuyi, G. Ung, High quantum yields from perfluorinated binolate erbium complexes and their circularly polarized luminescence, *J. Am. Chem. Soc.*, 2024, **146**, 7097–7104.
21. O. G. Willis, A. Pucci, E. Cavalli, F. Zinna, L. Di Bari, Intense 1400–1600 nm circularly polarised luminescence from homo- and heteroleptic chiral erbium complexes, *J. Mater. Chem. C*, *2023*, **11**, 5290–5296.
22. A. Sickinger, B. Baguenard, A. Bensalah-Ledoux, Y. Guyot, L. Guy, F. Pointillart, O. Cador, M. Grasser, B. Le Guennic, F. Riobé, O. Maury, S. Guy, Impact of the experimental bandwidth on circularly polarized luminescence measurements of lanthanide complexes: the case of erbium(III), *J. Mater. Chem. C*, 2024, **12**, 4253–4260.
23. O. G. Willis, F. Petri, G. Pescitelli, A. Pucci, E. Cavalli, A. Mandoli, F. Zinna, L. Di Bari, Efficient 1400–1600 nm circularly polarized luminescence from a tuned chiral erbium complex, *Angew. Chem. Int. Ed.*, 2022, **61**, e202208326.